Mesoporosity changes from cambium to mature tension wood: a new step toward the understanding of maturation stress generation in trees

Shan-Shan Chang, Françoise Quignard, Tancrède Alméras, Bruno Clair

Mesoporosity changes from cambium to mature tension wood: a new step toward the understanding of maturation stress generation in trees

Shan-Shan Chang[1], Françoise Quignard[2], Tancrède Alméras[1] and Bruno Clair[1,3]

[1]Laboratoire de Mécanique et Génie Civil (LMGC), CNRS, Université Montpellier 2, cc 048, Place E. Bataillon, 34095 Montpellier, France; [2]UMR 5253 CNRS-UM2-ENSCM-UM1, Institut Charles Gerhardt Montpellier, 8 rue de l'Ecole Normale, 34296 Montpellier Cedex 5, France; [3]CNRS, UMR Ecologie des Forêts de Guyane (EcoFoG), Campus Agronomique, BP 701, 97387 Kourou, France

Author for correspondence:
Bruno Clair
Tel: +594 0 594 32 03 05
Email: bruno.clair@cnrs.fr

Key words: cell wall maturation, maturation stress, mesoporosity, poplar *(Populus deltoides × P. nigra)*, tension wood.

Summary

- In order to progress in the understanding of mechanical stress generation, the mesoporosity of the cell wall and its changes during maturation of poplar (*Populus deltoides × P. nigra*) tension wood (TW) and opposite wood (OW) were measured by nitrogen adsorption–desorption.
- Variations in the thickness of the gelatinous layer (G-layer) were also measured to clarify whether the mesoporosity change simultaneously with the deposition of the G-layer in TW.
- Results show that mesoporous structures of TW and OW were very similar in early development stages before the deposition of G-layers. With the formation of the S_2 layer in OW and the G-layer in TW, the mesopore volume decreased steeply before lignification. However, in TW only, the decrease in mesopore volume occurred together with the pore shape change and a progressive increase in pore size.
- The different patterns observed in TW revealed that pores from G-layers appear with a different shape compared to those of the compound middle lamella, and their size increases during the maturation process until stabilising in mature wood. This observation strongly supports the hypothesis of the swelling of the G-layer matrix during maturation as the origin of maturation stress in poplar tension wood.

Introduction

Trees have a remarkable ability to modulate their secondary growth to adapt their material to environmental stresses (slope, wind, snow or light). More than just modifying the amount of secondary growth, trees can adapt the mechanical state of the wood produced. All around the circumference of the trunk, the newly formed wood layers are produced under tensile stress. Trees can develop a dissymmetry of the stresses around the tree circumference, generating a bending moment allowing the trunk to recover verticality or maintain a branch at a defined angle. In angiosperm trees, asymmetry is produced by forming a wood with high tensile stress, called tension wood, on the upper side of the leaning stem (Wardrop, 1964; Fisher & Stevenson, 1981). In tension wood, tensile stress is *c.* 5–10 times higher than in opposite wood (Archer, 1986; Fournier *et al.*, 1994; Clair *et al.*, 2013). The generation of this stress occurs during the maturation of the cell wall, and is therefore called maturation stress. This process may start after differentiation and elongation of meristematic fibres, as during these early stages the cell primary wall is too soft to support the stress. Then, stress generation is suspected to finish when the cell wall is stiff enough, possibly (but not surely) concomitant with the cell death.

In most of the temperate species, such as poplar, tension wood is characterized by the presence of gelatinous (G-) fibres which contain a peculiar cell wall layer, called the G-layer (Onaka, 1949; Dadswell & Wardrop, 1955) replacing the S_3 and part or whole of the S_2 layer. The G-layer is highly cellulosic with highly crystalline cellulose and microfibrils oriented nearly parallel to the fibre axis (Fujita *et al.*, 1974; Daniel *et al.*, 2006). Cellulose microfibrils are embedded within a matrix of polysaccharides, including pectin (Bowling & Vaughn, 2008), xyloglucan (Nishikubo *et al.*, 2007), glucomannan and xylan (Kim & Daniel, 2012) and arabino-galactan proteins (AGP; Lafarguette *et al.*, 2004; Andersson-Gunneras *et al.*, 2006; Bowling & Vaughn, 2008). A strong activity of a xyloglucan transglucosylase/hydrolase (XTH) was also reported in the G-layer (Nishikubo *et al.*, 2007; Mellerowicz *et al.*, 2008; Hayashi & Kaida, 2010). Contrary to any other secondary wall, the G-layer is almost devoid of lignin (Pilate *et al.*, 2004; Yoshinaga *et al.*, 2012).

In many tropical tree species, tension wood does not contain any G-layer, showing that the G-layer is not always necessary for

the generation of tensile maturation stress. Nevertheless, the G-layer has been taken as a model for studying the origin of maturation stress. Indeed, in species in which it is present, the G-layer is recognised as playing an essential role in the mechanism of stress generation in tension wood. First evidence comes from the relationship between the amount of G-layer and the stress level: the higher the amount of G-layer, the higher the tensile stress (Clair *et al.*, 2003; Yamamoto *et al.*, 2005; Fang *et al.*, 2008). It has been suggested (Münch, 1938; Goswami *et al.*, 2008) that the G-layer was providing the initial driving force generating this stress, which would be transferred to outer lignified layers and finally supported by them. However, observation at the cell wall level of the high contractile deformation of the G-layer when a free surface is created in a tension wood sample (Clair *et al.*, 2005), proves that the G-layer is not only the driver of, but also supports the tensile stress. Finally, the observation of the cellulose lattice spacing changes in the fibre direction using synchrotron X-ray diffraction during stress release (Clair *et al.*, 2006) and following the maturation process (Clair *et al.*, 2011), revealed that tensile stress is directly supported by cellulose microfibrils and that the stress is generated synchronously with the synthesis of the G-layer in poplar tension wood.

However, the mechanism of maturation stress generation still remains to be addressed: what generates this tension inside G-layer microfibrils? Different hypotheses have been proposed and discussed to explain this mechanism towards elucidating G-layer functions: the modification of the cellulose structure (Bamber, 2001; Mellerowicz *et al.*, 2008), the contraction of amorphous zones within the cellulose microfibrils (Okuyama *et al.*, 1994; Yamamoto, 2004), or the biochemical activity of hemicellulose in the G-layer matrix during the formation of microfibril aggregates (Nishikubo *et al.*, 2007; Bowling & Vaughn, 2008; Mellerowicz *et al.*, 2008). Alméras *et al.* (2012; later detailed by the authors in Fournier *et al.*, 2014) proposed several mechanisms whereby the stress would be transferred to the cellulose microfibrils by the swelling or shrinkage of the matrix in an interconnected network of cellulose microfibrils. The hydrophilic properties of gels could provide a physical basis for the cause of this matrix swelling or shrinkage.

From a physicochemical point of view, hydrogels are defined by a large amount of water-filled mesopores (with cavities from 2 to 50 nm across). The nitrogen adsorption method allows estimation of the pore size and surface area of mesoporous materials (Gregg & Sing, 1982; Rouquerol *et al.*, 1999). This technique is based on the measurement of the adsorption isotherm of N_2 at its boiling temperature (77 K) on an outgassed sample. The analysis of the isotherm allows for the determination of the amount of N_2 used for the deposition of the first monolayer (giving the surface area) and the following N_2 layers up to the filling of the pores. Knowledge of the size of N_2 molecules allows for determination of pore size distribution. A detailed description of the method applied to wood is given in Chang *et al.* (2009). This technique applied to the study of the texture of tension wood aerogel allowed for the identification of the hydrogel structure of the G-layer characterized by a large amount of water-filled mesopores, with peak-pore size ranging from 6 to 12 nm in chestnut (*Castanea sativa*) tension wood (Clair *et al.*, 2008), poplar tension wood (Chang *et al.*, 2011, 2012) and in several tropical species (Chang *et al.*, 2009).

Gels are known to be able to exhibit high shrinkage or swelling in response to physicochemical changes, such as ion concentration change. In angiosperm, similar cellulose-based hydrogels have been shown in the pit membranes of vessels and it has been proposed that the microstructure change depends on the change of cation concentration (Zwieniecki *et al.*, 2001; van Ieperen, 2007; Lee *et al.*, 2012). Therefore, physicochemical changes of pectin-like substances in the G-layer matrix could make it swell or shrink and then be the driving force of the growth stress generation in tension wood. These strains are expected to be accompanied by changes in pore size and/or shape in the gel of the G-layer. The aim of this study is to follow these changes during the maturation process of poplar tension wood.

In this study, wood tissues were sampled at different depths from the cambium to mature wood on the upper side (tension wood) and the lower side (opposite wood) of a naturally tilted poplar tree. The mesoporous texture of the samples, in their aerogel forms, was analysed using the nitrogen sorption isotherm technique in order to record the changes in shape and size of mesopores during wood formation, and check the assumption of G-layer matrix swelling or shrinkage during maturation stress generation. Opposite wood was taken as a control, as usual in studies of tension wood, because 'normal' woods (taken in a straight stem or in lateral sides of a tilted stem) may contain a small amount of G-layers, which could have a confounding effect on the results.

Materials and Methods

Sampling

A naturally tilted poplar (*Populus deltoides* (Bartr.) Marsh. × *P. nigra* L.) tree (24 cm diameter at breast height (dbh)) grown in Grabels (Domaine Maspiquet, Lycee Agropolis Montpellier) in the South of France was sampled on 7 June 2012 during a fast growing period. The tree was felled at 11:00 h and sampling was performed early in the afternoon at the laboratory. The sampling was made on both the upper side (tension wood) and the lower side (opposite wood) of the leaning stem according to the procedure described below. The bark and phloem were carefully removed to open a 'window' to the cambial zone (Fig. 1a). For the bark side, the inner surface of the phloem was peeled with knife blade and the peeled sample was marked as T0 and O0, respectively, for tension side and opposite side. For the xylem side, the back of a scalpel blade was used to peel the entire surface gently, and the first peeled sample was marked as T1 and O1. For the second and third peeled samples (numbered T2, T3, O2 and O3), the front of a scalpel blade and a knife blade were used, respectively, with increasing peeling force while carefully avoiding sectioning. Peeling of the soft tissues of the developing xylem result in a highly hydrated fibrous material indicating that the peeling separates fibers but does not (or does so only marginally) break the cell walls. Some resultant stretching is expected at a micrometric scale but this is assumed not to affect significantly the

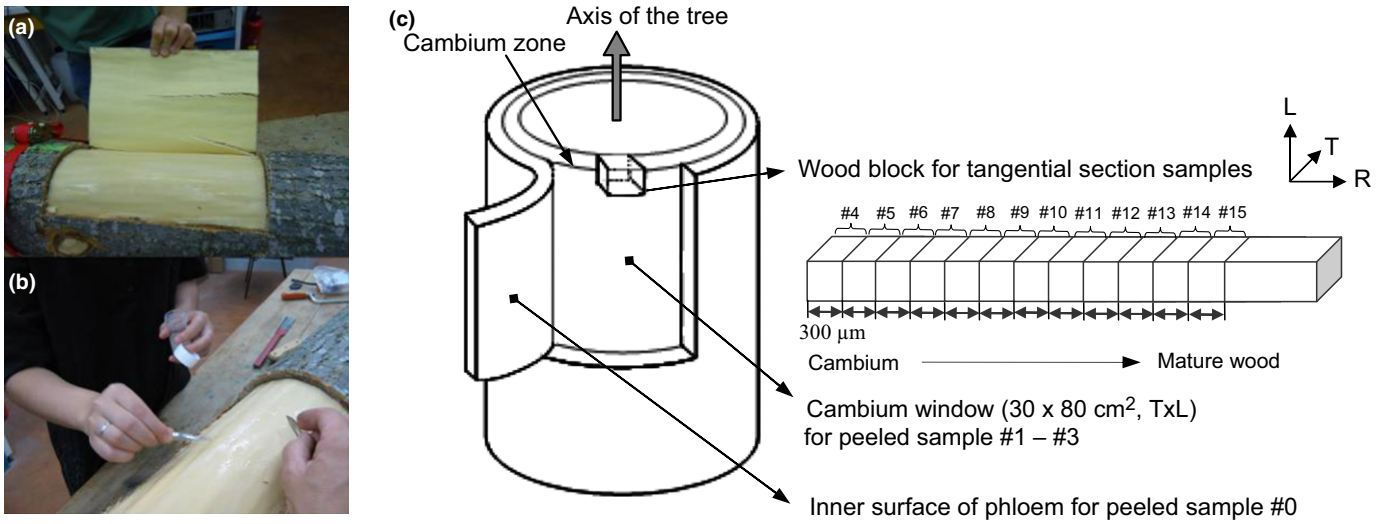

Fig. 1 Picture of the peeling experiment. (a) Debarking. (b) Peeling of the soft first wood layer (T1). (c) Schematic diagram showing sample preparation for N_2 adsorption–desorption measurement to examine the mesoporosity from each developmental stage of poplar (*Populus deltoides* × *P. nigra*) tension wood cell wall formation (tension wood side taken as example). L, longitudinal direction; R, radial direction; T, tangential direction.

mesoporosity, which is at a nanometric scale. After three peeled samples, it becomes impossible to obtain further samples by peeling due to the increasing adherence between fibers. Then wood blocks ($20 \times 10 \times 10$ mm, longitudinal (L) × tangential (T) × radial (R)) were extracted from the peeled area with care to avoid mechanical damage and maintain samples in a wet condition during the time of sampling. Then 260-µm-thick samples (obtained with several sections) were cut successively from the wood blocks with a sliding microtome until the previous growth ring was reached. In total 12 sectioned samples for the tension wood side, numbered T4–T15 and nine sectioned samples for the opposite wood side, numbered O4–O12, were obtained. Immediately after peeling and sectioning, samples were kept in 30% ethanol and dehydrated in a graded series of ethanol solutions (30%, 50%, 70%, 85%, 96% and 100%). The dehydrated samples were exchanged with liquid CO_2 and supercritically dried (aerogel form) before N_2 adsorption measurements in order to maintain the mesoporosity, avoiding the collapse of the gel (Clair *et al.*, 2008).

Several previous works (Clair *et al.*, 2008; Chang *et al.*, 2009, 2011, 2012) have shown the reproducibility of the measurements in mature tension wood and opposite wood and the strong difference of mesoporosity between these types. Here the aim of the study is to make a detailed description of the changes in mesoporosity from cambium to mature wood, so the choice was therefore to maximize the number of steps on a single tree by refining the sample thickness for each step for both tension wood and opposite wood formation. In order to check the reproducibility in the developing xylem, other poplar trees were sampled in the cambial zone (S. S. Chang, unpublished data) and results were in good agreement with presented data. Part of the samples were also duplicated in order to validate the repeatability of our measurements, and here again, results were in perfect accordance.

The distance from the cambial zone was recorded for each tangential section. For peeled samples, a small wood block was sampled before the first peeling and after each peeling, at which point the distance from the border of the block to the annual ring was measured with ImageJ (National Institutes of Health, Bethesda, MD, USA) in order to estimate the depth of successive peelings.

Microscopic observations and cell wall thickness measurement

Wood blocks extracted from unpeeled samples at the vicinity of the peeled part were dehydrated with ethanol and embedded in LR White resin (two exchanges of resin/ethanol mixture for 1 h, followed by two exchanges in pure resin for 1 h and kept overnight at room temperature, then polymerised at 65°C overnight). Transverse sections of 1-µm thickness were cut with a diamond knife and observed with an optical microscope (Leica Microsystems, Milton Keynes, UK) in phase contrast mode. The radial cell wall thicknesses (with and without G-layer) were manually measured from the images using the image analysis software ImageJ. Measurement of cell wall thicknesses without the G-layer allows calculation of the non-G-layer cell wall (called other layers, OL), and measurement of thicknesses with the G-layer allows calculation of the G-layer thickness (GL) by subtracting OL.

N_2 adsorption–desorption measurement

The supercritically dried samples (*c.* 0.4–0.7 g) were outgassed at 323 K under vacuum until a stable 3×10^{-5} Torr pressure was reached without pumping. This is done to remove physically adsorbed gases from the sample surface, in particular, water vapour. Nitrogen adsorption–desorption isotherms were recorded at 77 K on a micromeritics ASAP 2020 volumetric apparatus.

This experimental technique allows evaluating the surface area (S_{BET}, Brunauer *et al.*, 1938) which is directly correlated with the pore volume (Gregg & Sing, 1982) and the pore size distribution

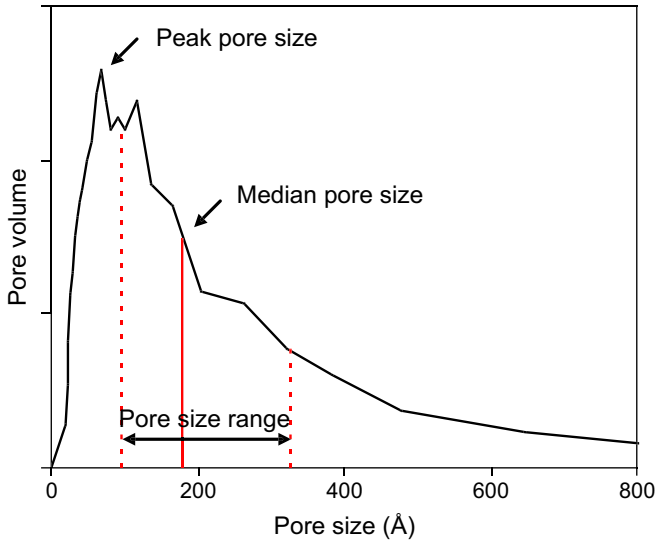

Fig. 2 Representation of the median pore size and pore size range in poplar (*Populus deltoides* × *P. nigra*) calculated from the adsorption pore size distribution (using method of Broekhoff & de Boer, 1967). Fifty percent of the pore volume has a pore size in between the two vertical dotted lines (25% and 75%). The plain vertical line represents the median pore size (50%).

(Broekhoff & de Boer, 1967) of the samples. In order to characterise the change in the whole distribution of pore sizes, pore size is not only characterised by its peak pore size (size of the pores the more represented), but also by its range of distribution. The pore size range was calculated from adsorption pore size distribution diagrams (Fig. 2) after integration of the area under the curve of pore size distribution. Corresponding pore sizes at 25%, 50% (median) and 75% of the volume were then plotted for each peeling or section sample (Figs 3c, 4c).

Under the assumption of a uniform distribution of pores in the material, an average pore diameter (D) and a distance between pores (t) can be estimated using surface (S_{BET}) and mesopore volume (V_{mp}):

$$D = X \times V_{mp}/S_{BET} \quad \text{Eqn 1}$$

with $X = 2$, 3 or 4 depending on the pore shapes spherical, cylindrical or lamellar, respectively;

$$t = 2/(S_{BET} \times \rho) \quad \text{Eqn 2}$$

with $\rho \approx 1.5$ for wood constituents. The hypothesis of an uniform porosity of the cell wall is only acceptable near the cambial zone, before the deposition of the secondary wall, and therefore these parameters are only used to discuss the early change of mesoporosity near cambial zone.

Results

Cell wall deposition

Figures 3(b) and 4(b) show variations in the average thickness of cell wall layers during maturation of opposite wood and tension wood, respectively. The thicknesses are plotted vs the distance of the measured fibres from the cambial zone. In Figs 3(a) and 4(a) light micrographs of the transverse sections of opposite wood and tension wood, respectively, are shown, displaying the cell differentiation at different distance from the cambium. These photographs demonstrated that the optical microscopy in phase contrast mode allows one to easily trace G-layer formation from unstained transverse sections.

In the first 500 µm after the cambium, the gradual thickening of the compound middle lamella (CML) and secondary wall layer is clearly visible both in opposite wood and tension wood (Figs 3a1–a3, 4a1–a2). No difference in cell morphology between opposite wood and tension wood could be observed in this area. In opposite wood, the thickening of the cell walls is completed at 1100 µm after the cambium where the cell wall thickness remains constant (Fig. 3a5–a6). No G-layer was observed in the opposite wood sample (Fig. 3a). In tension wood, the G-layers start to become visible after 500 µm (Fig. 4a3). However, the sudden decrease of OL thickness at the same position suggests that a very thin G-layer could already be produced at *c.* 400 µm (the dotted line in Fig. 4b is an interpolation of the G-layer thickening) but is not detectable when its thickness is < 0.3 µm.

The G-layer thickness changes abruptly at the growth ring transition located *c.* 2600–2800 µm (Fig. 4b). This change can be attributed to the decrease in fibre diameter in latewood and the strong relationship between G-layer thickness and fibre diameter, as observed in poplar by Fang *et al.* (2008). In tension wood, OL thickness is not disturbed at the ring transition. In opposite wood, a sharp change of the cell wall thickness is observed at the growth ring transition *c.* 2300–2400 µm (Fig. 3b).

High mesoporosity in the cambial zone and its sudden loss after the last peelable sample

The surface area S_{BET} of the samples from opposite wood and tension wood are shown in Figs 3(c) and 4(c), respectively. The value of S_{BET} is very high near the cambium zone allowing us to conclude that the middle lamella and primary wall (hereafter denoted CML) have a hydrogel structure in the early stages of wood formation. During these stages, the wall is made of an unorganised cellulose network embedded in hemicelluloses and pectin components which are known for their ability to produce a gel. These 'wood' layers are weakly bonded to each other and were easily manually peeled.

After this stage, the surface area of opposite wood decreases dramatically until it almost disappears (1.2–1.5 $m^2 g^{-1}$), parallel to the linear increase in cell wall thickness. In tension wood, the steep decrease of surface area starts from sample T3 at 105 $m^2 g^{-1}$ to sample T5 at 11 $m^2 g^{-1}$ and then remains constant, due to the appearance of the G-layer from T4. At positions O4 and T4, the cohesion between fibres is much stronger and prevented sample preparation by peeling, indicating also some strong modification in the CML. At this stage, the cell wall reaches about half of its final thickness in opposite wood, whereas in tension wood, OL nearly reached its final thickness and the G-layer is presumably starting to be deposited.

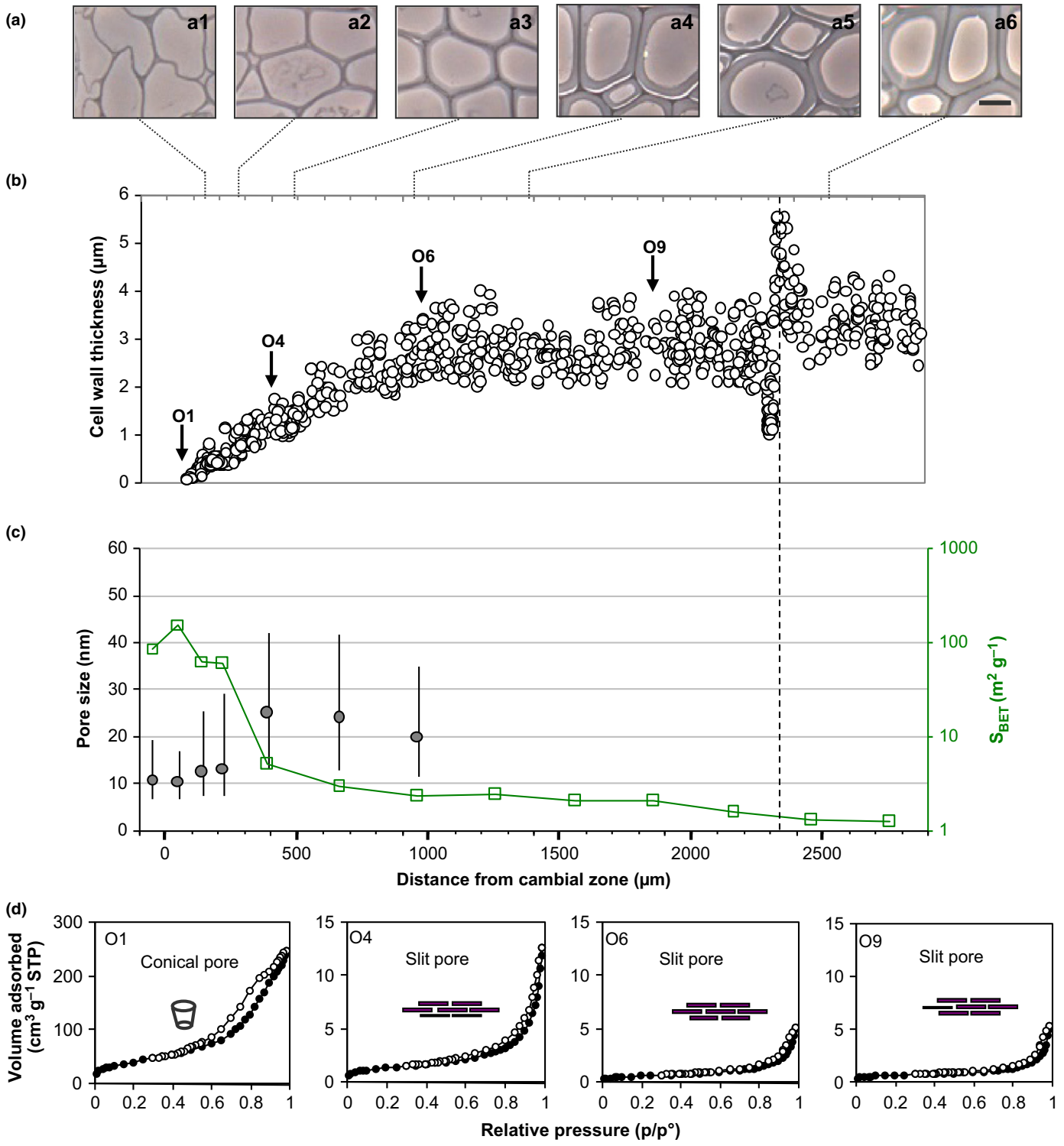

Fig. 3 Cell wall structure and mesoporous texture of poplar (*Populus deltoides* × *P. nigra*) opposite wood during cell wall maturation. (a) Morphological fibre details according to the distance from the cambial zone in poplar opposite wood. Bar, 10 µm. The light micrographs (a1–a6) were acquired with an optical microscope in phase contrast mode. (b) Cell wall thickness. (c) Median pore size (closed circles), pore size range (straight lines) and surface area (open squares, S_{BET}, displayed in logarithmic scale). The vertical dashed line indicates the position of the previous growth ring. (d) Nitrogen sorption isotherms at four key stages: O1, early stage of cell wall thickening; O4, later stage of cell wall thickening; O6, completion of cell wall thickening; O9, mature cell wall (closed circles, adsorption; open circles, desorption; the corresponding pore shapes are presented in each figure). STP, standard temperature and pressure (0°C, 100 kPa).

Table 1 shows the D and t under the assumption of an uniform pore distribution. In opposite wood, the transition between O3 and O4 is characterized by a decrease in D but also an overall steep increase in t. This increase by a factor > 10 cannot be attributed to the change in pore size and can only be the result of the filling of almost all the mesoporosity, indicating that

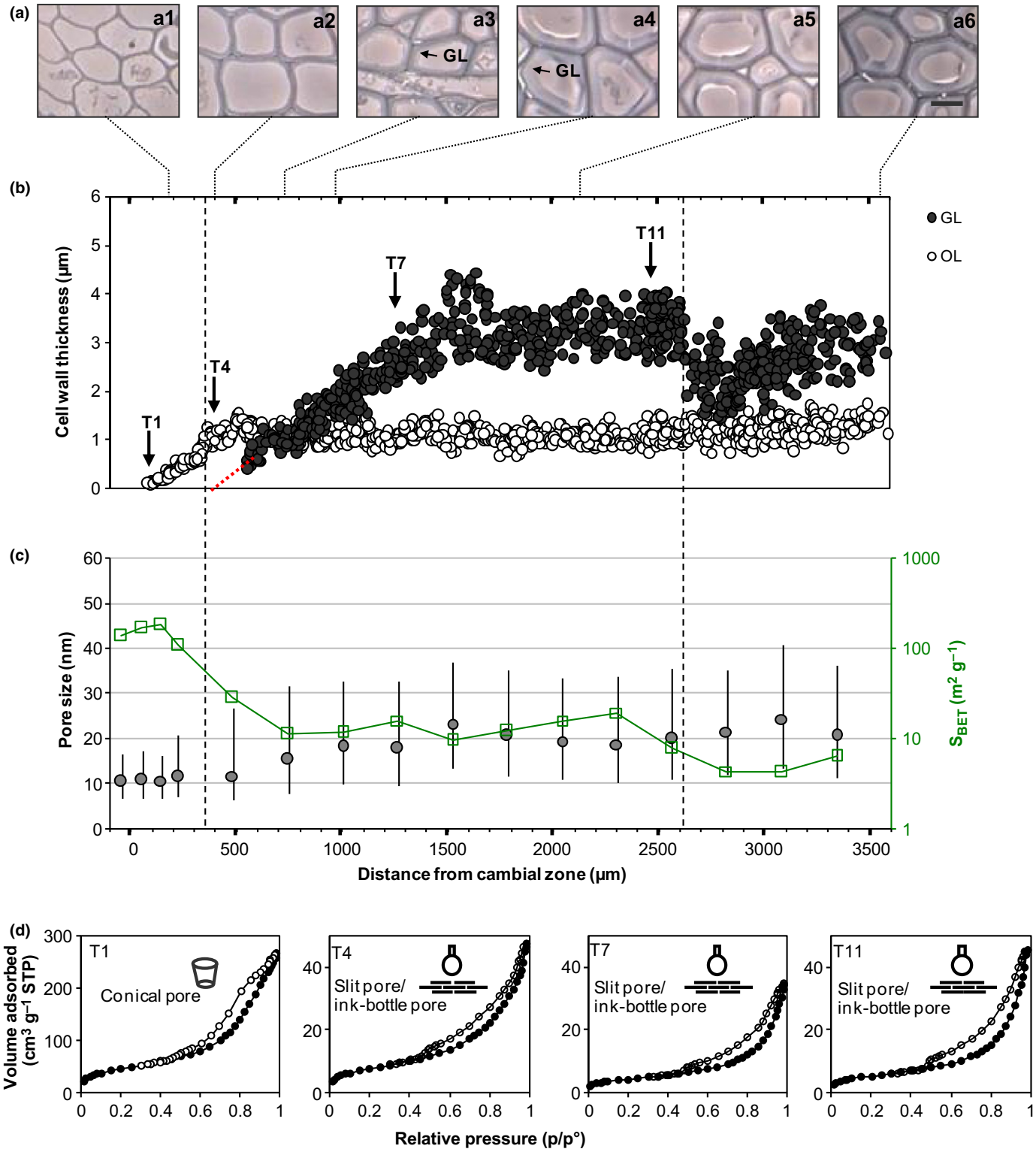

Fig. 4 Cell wall structure and mesoporous texture of poplar (*Populus deltoides* × *P. nigra*) tension wood during cell wall maturation. (a) Morphological fibre details according to the distance from the cambial zone. Bar, 10 µm. The light micrographs (a1–a6) were acquired with an optical microscope in phase contrast mode. (b) Cell layer thickness. GL, gelatinous (G-) layer (closed circles); OL, sum of all other layers in cell wall except G-layer (open circles). The red dotted line is an interpretation of the G-layer thickening when its thickness is not yet detectable. (c) Median pore size (closed circles), pore size range distribution (straight lines), and surface area (open squares, S_{BET}, displayed in logarithmic scale). (d) Nitrogen sorption isotherms at four key stages: T1, before G-layer formation; T4, early stage of G-layer formation; T7, later stage of G-layer formation; T11, after completion of G-layer thickening (closed circles, adsorption; open circles, desorption; the corresponding pore shapes are presented in each figure). Vertical dashed lines at 350 µm where the G-layer is supposed to appear; the vertical dashed line around 2600 µm was the previous growth ring. STP, standard temperature and pressure (0°C, 100 kPa).

Table 1 Pore size diameter (*D*) and distance between pores (*t*) calculated from surface (S_{BET}) and and mesopore volume (V_{mp}) under the assumption of an uniform distribution of cylindrical pore in the poplar (*Populus deltoides* × *P. nigra*) material

	Peeled samples			Sections	
	1	2	3	4	5
D (nm)					
OW	7.8	6.8	6.2	2.6	2.2
TW	7.9	8.3	7.6	6.0	6.4
t (nm)					
OW	8.7	21.5	22.9	265.8	462.0
TW	7.7	7.1	11.8	44.5	108.8

OW, opposite wood; TW, tension wood. Abrupt change in *t* from peeled sample to section cannot be explained by the *D* increase indicating the filling of most of the mesoporosity between the stages.

the middle lamella and primary wall lose there porosity before the completion of the cell wall. This deposition of new material in the mesoporous system would explain the difference in attachment/cohesion between fibres observed during sampling ('peelable' to 'unpeelable'). In tension wood, a similar trend is observed but additional mesoporosity from the newly deposited G-layer makes the transition less abrupt. However, considering the sample preparation, wherein these two states of the wall could clearly be separated, it can be stated that in tension wood, also, mesoporosity from the CML is mainly filled when deposition of the G-layer starts.

Pore shape

The shape of the N_2 adsorption–desorption isotherms combined with the difference in pore size distributions obtained from adsorption and desorption provide information on the shape of the pores in the samples (Groen & Pérez-Ramirez, 2004). Isotherms are compared at all stages during cell differentiation of tension wood and opposite wood; only four stages are presented in Figs 3(d) and 4(d) (full set of data is presented in Supporting Information Figs S1, S2). For opposite wood, the selection of the four stages was defined as follows: O1, early stage of cell wall thickening; O4, later stage of cell wall thickening; O6, completion of cell wall thickening and O9, mature cell wall. For tension wood, the selection of the four stages was based on the G-layer formation: before G-layer formation (T1), early stage of G-layer formation (T4), later stage of G-layer formation (T7) and completion of G-layer thickening (T11). Measurements at other locations showed similar isotherms for each differentiation stages.

According to the International Union of Pure and Applied Chemistry (IUPAC) classification (Sing *et al.*, 1985), the isotherms of tension wood are type IV with a H3 type hysteresis loop, indicating the presence of mesopores with a nonuniform size. For opposite wood, the isotherm of the first stage (O1) is similar with tension wood (T1). For the next three stages, the isotherms are intermediary between type IV and type II, indicating the presence of large mesopores with a broad size distribution that continues into the macropore domain. The hysteresis loop is very narrow, the adsorption and desorption branches being almost vertical and nearly parallel above 0.9 relative pressure.

Peak pore size determined from the adsorption branch of the isotherm corresponds to the cavity size, whereas that of the desorption branch corresponds to the throat size of a pore (Groen & Pérez-Ramirez, 2004). Thus, comparing the adsorption and desorption pore size distributions provides information about the pore shapes. At stage 1, for both tension wood and opposite wood, the peak pore size measured from the adsorption branch (7 nm) is smaller than the peak pore size measured from the desorption branch (8 nm). Both isotherms show a wide hysteresis loop between the adsorption and desorption branches ended near $p/p^\circ = 0.48$ with nearly parallel branches. This behaviour has been observed in adsorbents with highly connected three-dimensional pore systems (Fan *et al.*, 2001) and can be attributed to cone-shaped pores with a wide opening, which decreases the activation energy of condensation.

With the G-layer formation in tension wood, the desorption branch is characterised by a steep desorption at $p/p^\circ = 0.48$ in all isotherms, indicating that the pore opening is somewhat narrower than the pore cavity. The peak pore size calculated from desorption branches is still 8 nm, whereas more than one peak appears on the adsorption pore size distribution, with mean sizes of 7 and 12 nm. To produce such a size distribution, some of the pores have an ink-bottle shape with pore cavities that are less than twice the diameter of the throats, whereas others could have a slit-shape character with nearly constant cavity and throat sizes. The comparison of peak pore size from adsorption and desorption branches suggests that mesopores have an ink-bottle shape. This typical mesopore shape is characteristic of the G-layer as previously described in mature poplar (Chang *et al.*, 2011) and chestnut tension wood (Clair *et al.*, 2008). The transition from conical pores to ink-bottle shaped pores appears clearly between samples T3 and T4, indicating that a mesoporosity typical of the G-layer is already observed before the G-layer is visible in phase contrast microscopy.

For opposite wood, from O4 to mature wood, the hysteresis loops are very narrow, and the adsorption data show similar pore size to that of the desorption data (mean peak size of 8 nm). It tends to indicate the presence of mesopores between the cellulose microfibrils or in the matrix forming slit-shaped pores. However, it should be noted that due to the low mesopore volume and low surface area in opposite wood, the pore shape and pore size distributions have to be interpreted with caution.

Pore size distribution

Pore size ranges are shown in Figs 3(c) and 4(c) and a detail on some of the pore size distribution (determined from adsorption isotherm) is given in Fig. 5. Opposite wood and tension wood have very similar patterns near the cambium zone (at the first 300 μm after cambium) with median pore size *c.* 10 nm and peak pore size at *c.* 7 nm. Cell walls at this stage are mainly composed of the middle lamella and primary walls. After this stage, a new contribution of pores with peak pore size of 11.5 nm is observed in both opposite wood and tension wood (Fig. 5). The

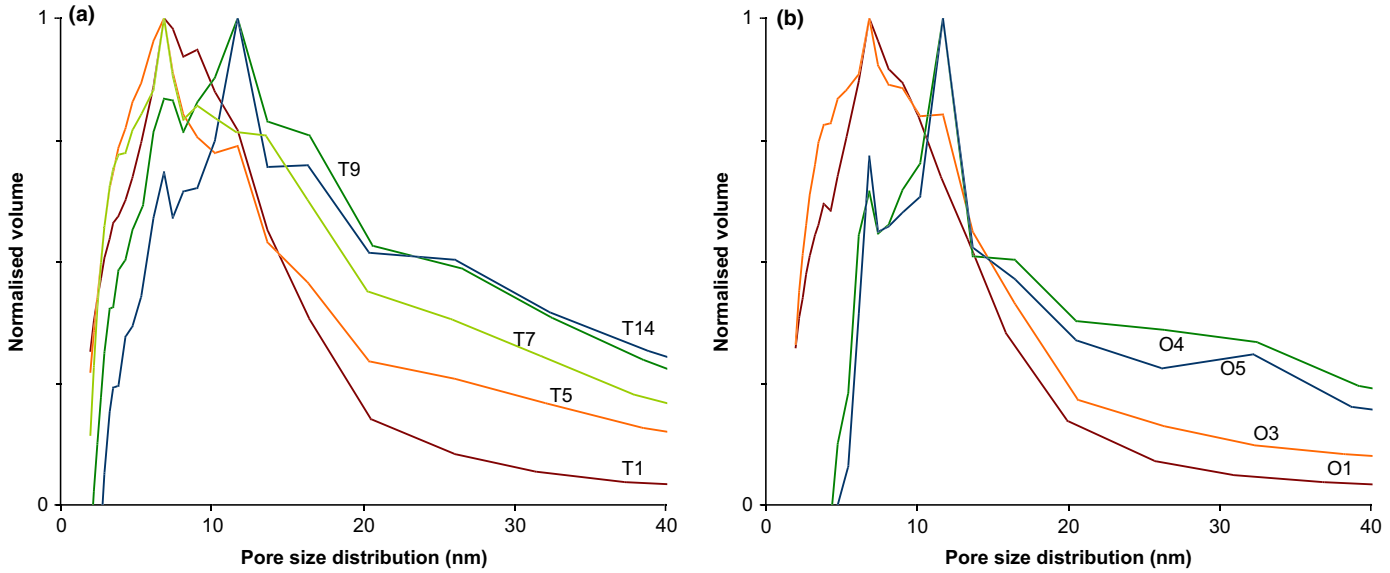

Fig. 5 Poplar (*Populus deltoides* × *P. nigra*) pore size distributions determined from the absorption branch of the isotherms of five of the samples from tension wood (a) and four of the samples from opposite wood (b). T1–T14 and O1–O5: tension wood and opposite wood samples, respectively, at increasing distance from cambium (T1, O1) to mature wood (T14, O5). Pore volume is normalised by its maximum value (value at peak pore size), in order to emphasize the shift in pore size during cell wall development, revealed by the decreasing contribution of the peak located near 7 nm, together with the increasing contribution of the peak located near 11.5 nm.

contribution of this peak increases during maturation to become higher than the peak at 7 nm at the end of the maturation process, both in opposite and tension wood (Fig. 5). This stage of cell maturation is also accompanied by an increasing median pore size and a wider pore range (Figs 3c, 4c). In tension wood, the pore size range progressively increases with a wider pore size range centred on 20 nm, nearly two times higher than in the cambial zone, synchronously with the deposition of the G-layer. This range remains nearly constant after the tension wood cell wall reaches its final thickness. In opposite wood, the median pore size increases much faster to reach *c.* 25 nm in sample O4 and sample O5. After 1000 µm, it becomes impossible to compute the pore size distribution in opposite wood due to the low volume of N_2 adsorbed close to the instrumental limitation.

Discussion

The N_2 adsorption–desorption isotherm method allowed for the characterisation of the mesoporosity changes during cell wall maturation in tension wood and opposite wood. The development of the CML started with the deposition of mesoporous material with high mesopore volume for both tension and opposite wood. The similar hysteresis loops indicate that tension wood and opposite wood both have a network of large-mouth conical pores in this development stage. With the cell wall thickening, the high porosity of the CML of opposite wood decreases abruptly and is nearly lost. This strong change indicates the deposition or reorganization of material in the wall. These modifications may be attributed to the lignification process. However, filling of the mesoporous system was found to occur much before the completion of the wall (about half of the final cell wall thickness), whereas Yoshinaga *et al.* (2012) observed on poplar with UV photographs and TEM micrographs after $KMnO_4$ staining that lignification of CML is not yet finished (especially between cell corners) when the cell wall is about half of its final thickness in normal wood (Yoshinaga *et al.*, 2007; A. Yoshinaga, pers. comm.) and in tension wood (Yoshinaga *et al.*, 2012). However, the detection by FTIR of a peak at 1500–1510 cm^{-1} attributed to the C=C (aromatic symmetrical stretching) of lignin (Marchessault, 1962; Faix, 1991) early in the cell wall deposition both in normal wood and tension wood (Chang *et al.*, 2014) may support the hypothesis that some precursor of lignin may be involved in the mesopore filling. The origin of the filling of the mesopores of the CML in this early stage of development remains therefore unsolved and would need a deeper investigation.

In tension wood the decrease of mesoporosity in the CML is compensated by a new mesoporosity, with ink-bottle shaped pores, changing the isotherm shape but maintaining the mesopore amount. This new mesoporosity, characterized by a pore shape typical of what was observed in the mature G-layer (Clair *et al.*, 2008; Chang *et al.*, 2009, 2011, 2012), is observable shortly before the G-layer was distinguished in phase contrast optical microscopy and remains all through the G-layer development until mature wood. This ink-bottle pore shape is never observed in opposite wood, even during the maturation process. However, the peak pore size is shifted from 7 to 11 nm in the early stage of maturation of opposite wood as it is in tension wood indicating that the mesoporous texture of secondary wall in opposite wood does not differ by the shape of pores but differs in pore size compared to the CML. In mature opposite wood, there was very low but detectable mesopore volume. This mesoporosity was proposed to be ascribed to the pit membranes of the vessels (Clair *et al.*, 2008; Chang *et al.*, 2009), which are known to be composed of unlignified primary wall with pectin gel as the

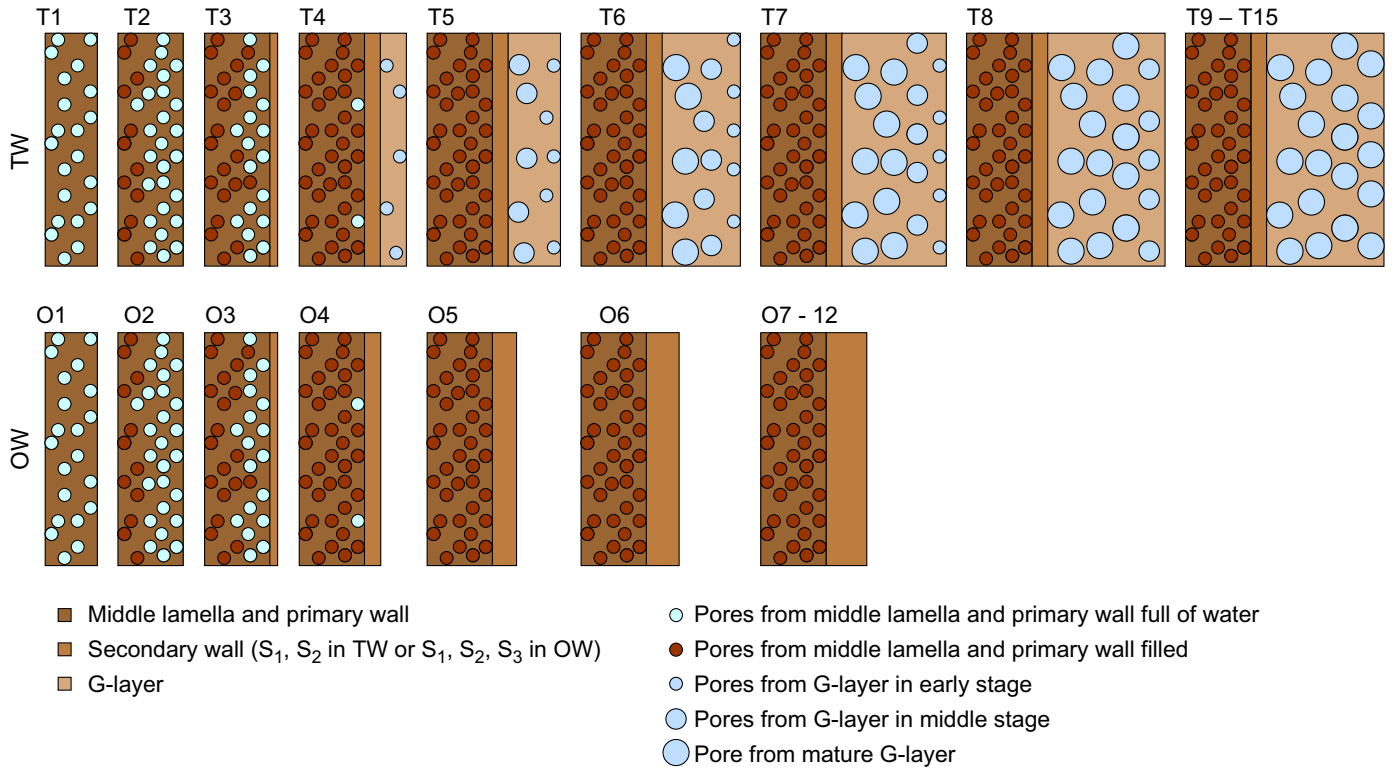

Fig. 6 Schematic drawing of the change in mesoporosity during maturation of the tension wood (TW) and opposite wood (OW) cell wall in poplar (*Populus deltoides* × *P. nigra*). T1–T15 and O1–O12: TW and OW samples, respectively, at increasing distance from cambium (T1, O1) to mature wood (T15, O12). Circles represent a mean pore size whereas it has been shown that a wide distribution of pore sizes are present. Cell wall layer thicknesses are not presented at a realistic scale in order to emphasize the mesoporous layers. Samples T1–T3 and O1–O3 were characterized by the light adherence between cells attributed to the weakness of the compound middle lamella allowing sampling by peeling, whereas other samples needed sectioning for preparation. G-layer, gelatinous layer.

G-layer (van Ieperen, 2007; Lee *et al.*, 2012). Interestingly, this mesoporosity is characterized by a pore size range wider than the G-layer and nearly three times wider than in primary wall of the same specimen. This would suggest that, if correctly attributed to the pits, the primary wall at the pit position would be modified during the maturation by enlarging the pores in order to achieve its conductive functions.

Most relevant to the understanding of maturation stress generation is the specific behaviour of mesoporosity during G-layer maturation. It appears that the pore size range increases progressively from a median value of 12 nm where first ink-bottle pores are visible (T4, *c.* 400 µm from the cambium) to *c.* 20 nm at 1600 µm away from the cambium when the G-layer thickness remain stable and the G-layer can be considered as mature. This increase in pore size is not sudden after G-layer deposition but starts from the early beginning of the G-layer deposition, suggesting a continuous increase in size of the newly deposited pores (see schematics Fig. 6). The initial size of pores in the G-layer is quite similar to the one observed in CML but differs by its shape, indicating that the initial state of G-layer matrix may present similar polysaccharides as in the CML but with a different organisation. This last observation could find explanation in the strong difference in the organisation of the cellulose network as CML have cellulose microfibrils much less organised than in the well orientated G-layer (Norberg & Meier, 1966).

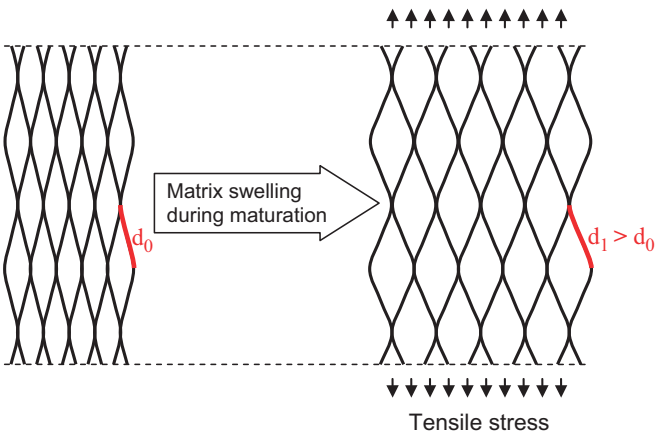

Fig. 7 Model of longitudinal tensile stress generation through the swelling pressure of the gelatinous matrix within the cellulose microfibril network.

The increasing pore size during maturation suggests that the G-layer matrix swells during cell wall maturation in tension wood. This observation strongly supports the hypothesis of a swelling of the matrix as the driving force of maturation stress generation as proposed by Alméras *et al.* (2012). According to this model (Fig. 7), the swelling of the matrix in the interconnected cellulosic network results in a longitudinal stress of high magnitude, through the redirection of the swelling pressure along

the microfibrils, thus putting them in a state of tensile stress, consistent with *in vivo* observations of the extension of cellulose lattice spacing during G-layer maturation (Clair *et al.*, 2011).

Future lines of research on this topic will focus on the triggers of this swelling. It is known that some physicochemical changes such as water content or ion concentration, as observed in pit membranes (van Ieperen, 2007; Lee *et al.*, 2012), are able to act on the gel structure and function. However, up to now, no evidence has been provided that a similar process occurs during maturation of tension wood cell wall. Another challenge will be to elucidate the mechanisms associated with tension stress generation in species not producing a G-layer.

Acknowledgements

S-S.C. was supported by a fellowship from the Scientific Council of Montpellier University. The authors wish to thank Francesco Di Renzo (ICG Montpellier) for valuable discussions. P. Brunier from Domaine Maspiquet in Grabels (Lycee Agropolis Montpellier) for the poplar tree used for this study. Part of this work was performed in the framework of the project 'StressInTrees' funded by the French National Research Agency (ANR-12-BS09-0004).

References

Alméras T, Gril J, Clair B. 2012. The origin of maturation stress in tension wood: using a wide range of observations and mechanical considerations to discriminate between hypothetic mechanisms. In: Moulia B, Fournier M, eds. *7th plant biomechanics international conference, Clermont-Ferrand, France*, 258.

Andersson-Gunneras S, Mellerowicz EJ, Love J, Segerman B, Ohmiya Y, Coutinho PM, Nilsson P, Henrissat B, Moritz T, Sundberg B. 2006. Biosynthesis of cellulose-enriched tension wood in *Populus*: global analysis of transcripts and metabolites identifies biochemical and developmental regulators in secondary wall biosynthesis. *Plant Journal* **45**: 144–165.

Archer RR. 1986. *Growth stresses and strains in trees.* Berlin, Germany: Springer.

Bamber RK. 2001. A general theory for the origin of growth stresses in reaction wood: how trees stay upright. *IAWA Journal* **22**: 205–212.

Bowling AJ, Vaughn KC. 2008. Immunocytochemical characterization of tension wood: gelatinous fibers contain more than just cellulose. *American Journal of Botany* **95**: 655–663.

Broekhoff JCP, de Boer JH. 1967. Studies on pore systems in catalysts: IX. Calculation of pore distributions from the adsorption branch of nitrogen sorption isotherms in the case of open cylindrical pores. A. Fundamental equations. *Journal of Catalysis* **9**: 8–14.

Brunauer S, Emmett PH, Teller E. 1938. Adsorption of gases in multimolecular layers. *Journal of the American Chemical Society* **60**: 309–319.

Chang SS, Clair B, Ruelle J, Beauchêne J, Di Renzo F, Quignard F, Zhao GJ, Yamamoto H, Gril J. 2009. Mesoporosity as a new parameter in understanding of tension stress generation in trees. *Journal of Experimental Botany* **60**: 3023–3030.

Chang SS, Hu JB, Clair B, Quignard F. 2011. Pore structure characterization of poplar tension wood by nitrogen adsorption–desorption method (*in Chinese with English abstract*). *Scientia Silvae Sinicae* **47**: 134–140.

Chang SS, Salmén L, Olsson A-M, Clair B. 2014. Deposition and organisation of cell wall polymers during maturation of poplar tension wood by FTIR microspectroscopy. *Planta* **239**: 243–254.

Chang SS, Quignard F, Di Renzo F, Clair B. 2012. Solvent polarity and internal stresses control the swelling behavior of green wood during dehydration in organic solution. *Bioresources* **7**: 2418–2430.

Clair B, Alméras T, Pilate G, Jullien D, Sugiyama J, Riekel C. 2011. Maturation stress generation in poplar tension wood studied by synchrotron radiation micro-diffraction. *Plant Physiology* **155**: 562–570.

Clair B, Alméras T, Yamamoto H, Okuyama T, Sugiyama J. 2006. Mechanical state of native cellulose microfibrils in tension wood. *Biophysical Journal* **91**: 1128–1135.

Clair B, Alteyrac J, Gronvold A, Espejo J, Chanson B, Alméras T. 2013. Patterns of longitudinal and tangential maturation stresses in *Eucalyptus nitens* plantation trees. *Annals of Forest Science* **70**: 801–811.

Clair B, Gril J, Baba K, Thibaut B, Sugiyama J. 2005. Precautions for the structural analysis of the gelatinous layer in tension wood. *IAWA Journal* **26**: 189–195.

Clair B, Gril J, Di Renzo F, Yamamoto H, Quignard F. 2008. Characterization of a gel in the cell wall to elucidate the paradoxical shrinkage of tension wood. *Biomacromolecules* **9**: 494–498.

Clair B, Ruelle J, Thibaut B. 2003. Relationship between growth stress, mechanical-physical properties and proportion of fibre with gelatinous layer in chestnut (*Castanea sativa* Mill.). *Holzforschung* **57**: 189–195.

Dadswell HE, Wardrop AB. 1955. The structure and properties of tension wood. *Holzforschung* **9**: 97–104.

Daniel G, Filonova L, Kallas AM, Teeri T. 2006. Morphological and chemical characterisation of the G-layer in tension wood fibres of *Populus tremula* and *Betula verrucosa*: labelling with cellulose-binding module CBM1(HjCel7A) and fluorescence and FE-SEM microscopy. *Holzforshchung* **60**: 618–624.

Faix O. 1991. Classification of lignins from different botanical origins by FTIR spectroscopy. *Holzforschung* **45**: 21–27.

Fan J, Yu CZ, Wang LM, Tu B, Zhao DY, Sakamoto Y, Terasaki O. 2001. Mesotunnels on the silica wall of ordered SBA-15 to generate three-dimensional large-pore mesoporous networks. *Journal of the American Chemical Society* **123**: 12113–12114.

Fang CH, Clair B, Gril J, Liu SQ. 2008. Growth stresses are highly controlled by the amount of G-layer in poplar tension wood. *IAWA Journal* **29**: 237–246.

Fisher JB, Stevenson JW. 1981. Occurrence of reaction wood in branches of dicotyledons and its role in tree architecture. *Botanical Gazette* **142**: 82–95.

Fournier M, Alméras T, Clair B, Gril J. 2014. Biomechanical action and biological functions. In: Gardiner B, Barnett J, Saranpää P, Gril J, eds. *The biology of reaction wood. Springer series in wood science*. Berlin, Germany: Springer, 139–170.

Fournier M, Chanson B, Thibaut B, Guitard D. 1994. Measurement of residual growth strains at the stem surface. Observations of different species (*in French*). *Annals of Forest Science* **51**: 249–266.

Fujita M, Saiki H, Harada H. 1974. Electron microscopy of microtubules and cellulose microfibrils in secondary wall formation of poplar tension wood fibers. *Mokuzai Gakkai Shi* **20**: 147–156.

Goswami L, Dunlop JWC, Jungnikl K, Eder M, Gierlinger N, Coutand C, Jeronimidis G, Fratzl P, Burgert I. 2008. Stress generation in the tension wood of poplar is based on the lateral swelling power of the G-layer. *Plant Journal* **56**: 531–538.

Gregg SJ, Sing KSW. 1982. *Adsorption, surface area and porosity.* London, UK: Academic Press.

Groen JC, Pérez-Ramirez J. 2004. Critical appraisal of mesopore determination by adsorption analysis. *Applied Catalysis A: General* **268**: 121–125.

Hayashi T, Kaida R. 2010. Functions of xyloglucan in plant cells. *Molecular Plant* **4**: 17–24.

van Ieperen W. 2007. Ion-mediated changes in xylem hydraulic resistance in planta: fact or fiction? *Trends in Plant Science* **12**: 137–142.

Kim JS, Daniel G. 2012. Distribution of glucomannans and xylans in poplar xylem and their changes under tension stress. *Planta* **236**: 35–50.

Lafarguette F, Leplé JC, Déjardin A, Laurans F, Costa G, Lesage-Descauses MC. 2004. Poplar genes encoding fasciclin-like arabinogalactan proteins are highly expressed in tension wood. *New Phytologist* **164**: 107–121.

Lee J, Holbrook NM, Zwieniecki MA. 2012. Ion induced changes in the structure of bordered pit membranes. *Frontiers in Plant Science* **3**: 55.

Marchessault RH. 1962. Application of infra-red spectroscopy to cellulose and wood polysaccharides. *Pure and Applied Chemistry* **5**: 107–129.

Mellerowicz EJ, Immerzeel P, Hayashi T. 2008. Xyloglucan: the molecular muscle of trees. *Annals of Botany* **102**: 659–665.

Münch E. 1938. Statik und dynamik des Schraubigen baus der Zwellwand, besonders der druck- and zugholzes. *Flora* **32**: 357–424.

Nishikubo N, Awano T, Banasiak A, Bourquin V, Ibatullin F, Funada R, Brumer H, Teeri T, Hayashi T, Sundberg B *et al.* 2007. Xyloglucan endotransglycosylase (XET) functions in gelatinous layers of tension wood fibers in poplar – a glimpse into the mechanism of the balancing act of trees. *Plant Cell Physiology* **48**: 843–855.

Norberg PH, Meier H. 1966. Physical and chemical properties of the gelatinous layer in tension wood fibre of aspen (*Populus tremula* L.). *Holzforschung* **20**: 174–178.

Okuyama T, Yamamoto H, Yoshida M, Hattori Y, Archer RR. 1994. Growth stresses in tension wood: role of microfibrils and lignification. *Annals of Forest Science* **51**: 291–300.

Onaka F. 1949. Studies on compression and tension wood (translation from Japanese). *Wood Research* **1**: 1–88.

Pilate G, Chabbert B, Cathala B, Yoshinaga A, Leplé JC, Laurans F, Lapierre C, Ruel K. 2004. Lignification and tension wood. *Comptes Rendus Biologies* **327**: 889–901.

Rouquerol F, Rouquerol J, Sing K. 1999. *Adsorption by powders and porous solids: principles, methodology and applications.* San Diego, CA, USA: Academic Press.

Sing KSW, Everett DH, Haul RAW, Moscou L, Pierotti RA, Rouquerol J, Siemienewska T. 1985. Reporting physisorption data for gas/solid systems. *Pure and Applied Chemistry* **57**: 603–619.

Wardrop AB. 1964. The reaction anatomy of arborescent angiosperms. In: Zimmermann MH, ed. *The formation of wood in forest tree*. New York, NY, USA: Academic Press, 405–456.

Yamamoto H. 2004. Role of the gelatinous layer on the origin of the physical properties of the tension wood. *Wood Science and Technology* **50**: 197–208.

Yamamoto H, Abe K, Arakama Y, Okuyama T, Gril J. 2005. Role of the gelatinous layer on the origin of the physical properties of the tension wood of *Acer sieboldianum*. *Wood Science and Technology* **51**: 222–233.

Yoshinaga A, Kusumoto H, Laurans F, Pilate G, Takabe K. 2012. Lignification in poplar tension wood lignified cell wall layers. *Tree Physiology* **32**: 1129–1136.

Yoshinaga A, Wada M, Fujita M, Chabbert B, Pilate G. 2007. Modified lignification in the cell walls of CAD depressed poplars. *IAWA Journal* **28**: 457–471.

Zwieniecki MA, Melcher PJ, Holbrook NM. 2001. Hydrogel control of xylem hydraulic resistance in plants. *Science* **291**: 1059–1062.